ANALYSIS AND DESIGN OF A SERIES-PARALLEL RESONANT CONVERTER WITH CAPACITIVE OUTPUT FILTER

A K. S. Bhat, Senior Member IEEE,
Dept. of Electrical and Computer Engg.,
University of Victoria,
Victoria (B.C.)
V8W 2Y2
CANADA.

ABSTRACT :

A high-frequency link series-parallel resonant converter with capacitive output filter is proposed and analysed using state-space approach. Analysis shows that the converter enters into three different modes. The normalized load current and other component stresses are plotted against the converter gain. Detailed experimental results are presented to verify the theory.

1. INTRODUCTION

There are a number of possible high-frequency resonant converter configurations possible [1-6]. It has been shown by a number of authors that the series-parallel resonant converter (also called as "converter using LCC-type commutation" or as "LCC-type parallel resonant converter" or as "hybrid converter") [2, 5-13, 16,17] has a number of desirable features compared to series resonant or parallel resonant converter. Due to this reason, recently, there has been a considerable interest in this converter configuration [5-22]. It has been found suitable for a number of applications [6-13,17,18,21,22]. This type of converter uses inductive output filter similar to a conventional parallel resonant converter (PRC). Analysis of such converter has been presented by a number of authors [7-18]. Analysis presented in [7,10] uses Fourier series approach. A similar approach using complex circuit analysis is presented in [5,12,16,17]. State-space approach (or combined with state-plane diagrams) has been used for the analysis in [9, 13-15,18]. In all these papers, continuous capacitor voltage mode is assumed. However, recently it has been observed [18] that the series-parallel resonant converter also operates in discontinuous capacitor voltage mode which is similar to a conventional PRC [24].

It was first suggested by Steigerwald [23] that a conventional PRC can be operated with a capacitive output filter replacing the large filter inductor. This was further analysed in detail by Johnson and Erickson [24]. It is shown in this paper that a series-parallel resonant converter can also be operated with a capacitive output filter. It is shown that the analysis of such converter becomes extremely complex due to the presence of a number of modes and three intervals of operation. Analysis is presented for operation in both below (leading pf) as well as above resonance (lagging pf) mode. However, due to the advantages of operation above resonance, all the results and experiments will be concentrated for operation above resonance.

The objectives of this paper are to propose a LCC-type PRC with capacitive output filter, to present its different operating modes and to analyse the converter for these modes, to obtain design curves based on the analysis, then to present a simple design procedure for the proposed converter and finally to provide experimental results. These objectives are achieved in different sections of the paper as outlined below : Section 2 presents the basic operating principle of the converter and its different operating modes. The analysis of the proposed converter for different operating modes is presented in section 3 of the paper. Analysis is based on the state-space approach. Section 4 will present design curves obtained using the analysis presented in section 3. In the design curves, variable of interest is plotted against the normalized load current which simplifies the design. A simple design procedure is illustrated with a design example. Experimental results obtained with an experimental converter are presented in section 5.

2. OPERATING PRINCIPLE, OPERATING MODES AND MODELLING

Fig. 1 shows the basic circuit diagram of a series-parallel resonant converter (half-bridge version shown) with a capacitive output filter. It was observed that this converter enters into three different modes as the load current or switching frequency varies. Fig. 3 shows typical steady-state operating waveforms for the three different modes entered by the converter for operation above resonance. Similar modes exist for operation below resonance (with signs of i_{L0} and v_{ct0} reversed). Each mode of operation is characterized by different intervals of operation. Equivalent circuits during these different intervals are used for the analysis. For example, Fig. 2 shows the equivalent circuits for the three intervals of mode-1 operation.

Operation of the circuit in mode 1 can be understood by referring to the Figs. 1, 2 and 3(a) and is explained for the half-period when D1, S1 pair is active. During interval 1, the voltage across C_t is clamped to the output voltage $-V_o/n$ (referred to the primary-side). At the end of interval 1, resonating inductor current goes to zero and the rectifier diodes turn-off. This results in a resonating circuit comprising of L_s, C_s and C_t (Fig. 2(b)) and the voltage across C_t reverses from $-V_o/n$ to V_o/n. At the end of interval 2, when v_{ct} tries to increase above V_o/n, rectifier diodes begin to conduct clamping the voltage across C_t to V_o/n. This is represented by the equivalent circuit of Fig. 2(c) for the interval 3. Note that energy is supplied to the output only during the clamping intervals 1 and 2.

Mode 2 is an intermediate mode between the modes 1 and 3. There are only two intervals of operation for this mode (Fig. 3(b)). Models shown in Figs. 2(a) and (b) are applicable during these intervals.

Operation of mode 3 can be explained by referring to the waveforms shown in Fig. 3(c). In this case, operation begins with the equivalent circuit of Fig. 2(b) and then follows the sequence Fig. 2(a), and Fig. 2(b) again.

Analysis of the converter for the identifed modes and different intervals using the equivalent circuit models obtained is presented in the next section.

3. ANALYSIS

Detailed analysis of the converter using state-space approach for the three modes of operation explained above is presented in this section. Assumptions used in the analysis are stated in section 3.1. Analysis for modes 1, 2, and 3 are presented in sections 3.2, 3.3, and 3.4, respectively.

90/CH 2935-5/90/0000-1308$01.00©1990 IEEE

3.1 Assumptions Used : The following assumptions are used in the analysis.

(1) All the switches, diodes, inductors, capacitors and the hf transformer used are ideal.
(2) The output filter capacitor is large enough to assume that the load voltage is ripple-free.

3.2 Mode-1:

3.2.1 General Solutions: Typical operating waveforms for this mode are shown in Fig. 3(a). Using the equivalent circuit models for the three intervals shown in Fig. 2, and choosing the inductor current i_L, and capacitor voltages v_{cs} and v_{ct}, as the state variables, the state-space representation of the converter for this mode of operation is given by

$$[\dot{x}] = [A][x] + [B][u] \quad (1)$$

$$\text{where } [x] = [i_L \; v_{cs} \; v_{ct}]^T \quad (2)$$

$$[A] = \begin{bmatrix} 0 & -(1/L) & 0 \\ (1/C_s) & 0 & 0 \\ 0 & 0 & 0 \end{bmatrix} \text{ for intervals 1 and 3,} \quad (3)$$

$$[A] = \begin{bmatrix} 0 & -(1/L) & -(1/L) \\ 1/C_s & 0 & 0 \\ 1/C_t & 0 & 0 \end{bmatrix} \text{ for interval 2.} \quad (4)$$

$$[B][u] = [E+V_o/n \; 0 \; 0]^T \text{ for interval 1,} \quad (5)$$

$$= [E-V_o/n \; 0 \; 0]^T \text{ for interval 3,} \quad (6)$$

$$= [E/L \; 0 \; 0]^T \text{ for interval 2.} \quad (7)$$

Based on this state-space model, the normalized general solutions are obtained for the three different intervals and are given in Appendix 1. The following base quantities are used for the normalization:

$$V_B = E, \; Z_B = Z_s = (L_s/C_s)^{1/2}, \; I_B = V_B/Z_B \quad (8)$$

3.2.2 Steady-State Solutions : Using the general solutions obtained in section 3.2.1, steady-state solutions have been obtained by matching the boundary conditions of state variables at the end of each interval and using the condition that the values of state variables at the end of third interval are equal to, but, with opposite sign to those at t = 0. The normalized initial inductor current and the initial voltage across C_s thus obtained are given by

$$j_{L0} = [2\sin(\theta_3)\{-M(C_t/C_e) + \cos(\theta_1)\} + 2(C_e/C_s)^{1/2}\sin(\theta_{2e})\cos(\theta_1).\{M(C_t/C_e) + \cos(\theta_3)\}]/DR \quad (9)$$

$$1 + M - m_{cs0} = [-2 + 2\sin(\theta_1)\sin\{\theta_s - (\theta_1+\theta_2)\} + 2(C_e/C_s)^{1/2}\sin(\theta_1)\sin(\theta_{2e})\cos\{\theta_s-(\theta_1+\theta_2)\} - 2M(C_t/C_e)\{\cos\{\theta_s-(\theta_1+\theta_2)\} - (C_e/C_s)^{1/2}\sin(\theta_1)\sin(\theta_{2e})\}]/DR \quad (10)$$

$$\text{where DR} = -1 - \cos(\theta_s-\theta_2) + (C_e/C_s)^{1/2}\sin(\theta_{2e})\sin(\theta_s-\theta_2) \quad (11)$$

$$C_e = C_sC_t/(C_s + C_t) \quad (12)$$

$$w_s = 1/(L_sC_s)^{1/2}, \; w_e = 1/(L_sC_e)^{1/2} \quad (13)$$

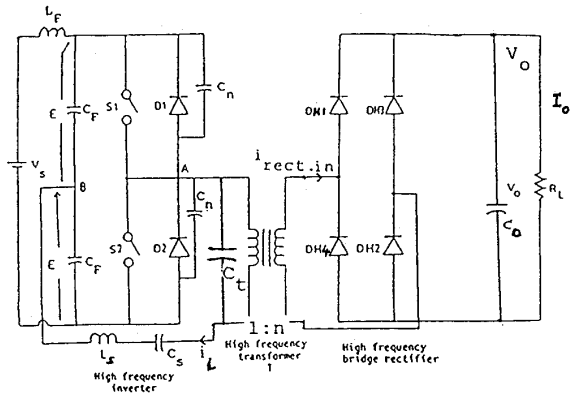

Fig. 1 Basic circuit diagram of LCC-type parallel resonant (Series-Parallel resonant) converter with a capacitive output filter, suitable for operation above resonance. (Switches S1 and S2 are high-frequency switches with gate or base turn-off capability)

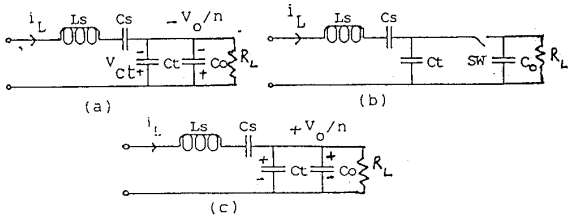

Fig. 2 Equivalent circuits during different intervals of operation for mode-1 operation. (a) Interval 1. (b) Interval 2. (c) Interval 3.

$$\theta_s = w_sT_s, \; \theta_1 = w_st_1, \; \theta_2 = w_st_2 \quad (14)$$

$$\theta_{1e} = w_et_1, \; \theta_{2e} = w_et_2 \quad (15)$$

$T_s = 1/(2f_t)$, f_t = switching frequency,

$$M = V_o/n \quad (16)$$

Also, it must be noted that for operation above resonance,

$$m_{ct0} = -M \quad (17)$$

In order to evaluate the initial conditions, it is necessary to calculate the duration of different intervals. For this purpose, the following constraints are used (refer to Fig. 3(a)):

$$j_{L1} = 0, \; m_{ct2} = M \quad (18)$$

The resulting equations are given below, which are solved numerically.

$$\cos(\theta_1) = M(C_t/C_e)[1 + \cos(\theta_s-\theta_2)\cos(\theta_{2e}) - (C_e/C_s)^{1/2}\sin(\theta_{2e})\sin(\theta_s-\theta_2)]/[1-\cos(\theta_{2e})] \quad (19)$$

$$\sin(\theta_1)[1 + \cos(\theta_s-\theta_2) - (C_e/C_s)^{1/2}\sin(\theta_{2e})\sin(\theta_s-\theta_2)] + \cos(\theta_1)\{-\sin(\theta_s-\theta_2) - (C_e/C_s)^{1/2}\sin(\theta_{2e})\cos(\theta_s-\theta_2)\} = -M(C_t/C_e)\{\sin(\theta_s-\theta_2) - (C_e/C_s)^{1/2}\sin(\theta_{2e})\} \quad (20)$$

$$t_3 = T_s - t_1 - t_2 \quad (21)$$

Once the duration of different intervals are known, the values of inductor current and capacitor volatges

at the end of different intervals can be obtained using the general solutions of Appendix 1.

3.2.3 Converter Gain on the Output Plane:

Under steady-state conditions, the average current through the output filter capacitor must be zero. Hence, since $i_L(t)$ flows to the output during intervals 1 and 3, the primary reflected load current can be written as

$$nI = (1/T_s)[-\int_0^{x_1} i_L(t)dt + \int_0^{x_3} i_L(t")dt"] \quad (22)$$

Using the equations (A1.1) and (A1.7), and simplifying, the normalized load current reflected to the primary side is given by

$$J = [2M(C_t/C_e)\{-1+\cos(\theta_3)\} + (j_{L0}/\sin(\theta_1))\{\cos(\theta_1) - 2 + \cos(\theta_3) - (C_e/C_s)^{1/2}\sin(\theta_{2e})\sin(\theta_3)\}]/(\theta_s) \quad (23)$$

This equation has been used to obtain the curves of gain M versus load current J for mode 1. These curves are drawn after the analysis of modes 2 and 3.

3.2.4 Peak Component Stresses

The expressions for the peak component stresses (peak inductor current and peak capacitor voltages) are derived below.

The time at which the inductor current reaches its peak value is dependent on it slope. It can be shown that the normalized inductor peak current is given by

$$J_{Lp} = j_{L0} \text{ p.u.} \quad -(m_{cs0}-M)<1 \quad (24)$$

$$= (C_e/C_s)^{1/2}\{1+M-m_{cs1}\} \text{ p.u.} \quad -(m_{cs0}-M)>1. \quad (25)$$

The voltage across C_s reaches its peak when i_L is zero. This occurs at the end of interval 1 and the value of normalized peak capacitor voltage is given by

$$m_{csp} = (1+M) -(1+M-m_{cs0}).\cos(\theta_1) + j_{L0}.\sin(\theta_1) \text{ p.u.} \quad (26)$$

The peak voltage across C_t is given by

$$m_{ctp} = M \quad \text{p.u.} \quad (27)$$

However, in practice, due to the diode drops and ripple in the load voltage, m_{ctp} will be higher than the value given by (27).

3.3 Mode-2

Fig. 3(b) shows typical operating waveforms for this mode of opeartion. This mode enters as the switching frequency is increased (or decreased - for below resonance) to regulate the output voltage. There are only two intervals for this mode of operation. The general solutions are presented in Appendix 2 and steady-state solutions have been obtained for this mode also. Mode 2 is an intermediate mode between the modes 1 and 3 and the solutions can also be obtained as a paticular case of mode 1.

In this mode since $i_L(t)$ flows to the output only during interval 2, the primary reflected normalized load current can be obtained from (23) with $\theta_3 = 0$.

The expressions for the peak component stresses (peak inductor current and peak capacitor voltages) are obtained as given for mode 1.

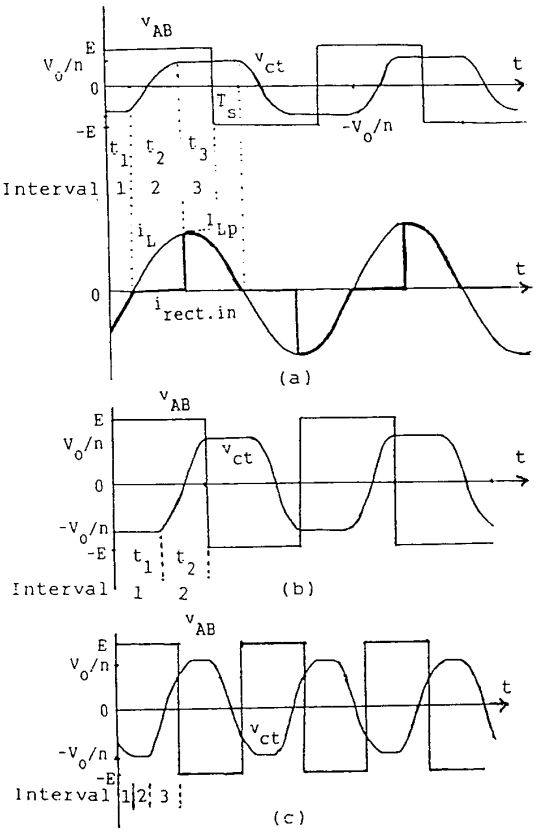

Fig. 3 Typical operating waveforms for three modes of operation.
(a) Mode-1. (b) Mode-2. (c) Mode-3.

3.4 Mode-3

Fig. 3(c) shows typical operating waveforms for this mode of operation. There are three intervals of operation. Using the equivalent circuit models shown in Figs. 2(a) and (b), state-space representation was obtained as done in section 3.2.1. The general solutions for this mode have been derived and they are presented in Appendix 3. Using the technique explained for mode 1, the following expressions are obtained for steady-state operation.

$$j_{L0} = -2(C_e/C_s)^{1/2}\{\cos(w_e t_1).\cos(w_s t_2) - (C_e/C_s)^{1/2}\sin(w_e t_1).\sin(w_s t_2)\}.\sin(w_e t_3)/DR3 \quad (28)$$

where $DR3 = 1 + \cos(w_s t_2)\cos(w_e(T_s-t_2)) - (C_e/C_s)^{1/2}\sin(w_s t_2)\sin(w_e(T_s-t_2))$ (29)

$$1-m_{cs0}-m_{ct0} = 2[1 - \{\sin(w_e t_1).\cos(w_s t_2) + (C_e/C_s)^{1/2}\cos(w_e t_1)\sin(w_s t_2)\}\sin(w_e t_3)]/DR3 \quad (30)$$

The value of m_{ct0} can be obtained using the condition $m_{cs3} = - m_{ct0}$. Therefore, m_{cs0} can be evaluated. To evaluate the above equations, the durations of three intervals must be calculated. Using the conditions $m_{ct1} = - M$ (value of m_{ct} at the end of interval 1) and $j_{L2} = 0$ (value of j_L at the end of interval 2), the following two equations are obtained. These two equations are solved numerically to obtain the values of θ_1 and θ_2. Then t_3 is given by (21).

$$(C_e/C_t)[(1-m_{ct0}-m_{cs0})[1-\cos(\theta_{1e})-\{\cos(\theta_{1e})\cos(\theta_2) - (C_e/C_s)^{1/2}\sin(\theta_{1e})\sin(\theta_2)\}(1-\cos(\theta_{1e}))] + j_{L0}[(C_s/C_t).(C_e/C_s)^{1/2}\sin(\theta_{1e}) + \{(C_s/C_e)^{1/2}\sin(\theta_{1e})\cos(\theta_2) + \cos(\theta_{1e})\sin(\theta_2)\}(1 - \cos(\theta_{3e})] - 2m_{ct1} = 0 \quad (31)$$

$$F_2 = \cos(\theta_{1e})\sin(\theta_2) + (C_e/C_s)^{1/2}\sin(\theta_{1e})\cos(\theta_2) - (C_e/C_s)^{1/2}\sin(\theta_{3e}) = 0. \quad (32)$$

The normalized load current can be obtained from

$$J = -[(C_e/C_s)^{1/2}(1-m_{cs0}-m_{ct0})\sin(w_e t_1) + j_{L0}\cos(w_e t_1](1-\cos(w_s t_2)/[(w_s T_s)\sin(w_s t_2)] \quad (33)$$

The peak component stresses are calculated using the same procedure as given in section 3.2.4.

It was found that mode-1 is the predominant mode. Modes 2 and 3 occur for higher frequencies of operation required to regulate the output voltage at light loads.

4. DESIGN

The analysis presented in section 3 is used to obtain the design curves for operation above resonance in this section. Fig. 4(a) shows the converter gain versus normalized load current for various values of y ($=2\pi f_t/w_s$) with a capacitor ratio of $C_s/C_t = 1$. Variation of normalized peak inductor current and the normalized peak voltage across C_s for variation in converter gain for various values of y are shown in Figs. 4(b) and (c) respectively. It was observed that for a given y, and if $y < (1+C_s/C_t)^{1/2}$, then the converter enters into below resonance mode as the load current is reduced below certain value. For values of y, greater than the above value, converter is always in the above resonance mode and enters mode 3 at light loads. For a given y and for a given load current, output load voltage and component stresses can be directly read from the graphs of Fig. 4. Note that in Fig. 4(a), points on the M axis correspond to open circuit condition, whereas, points on the J axis represent load short circuit operation.

Design procedure is illustrated below by a design example.

The converter has the following specifications.

Power output, $P_o = 500$ W,
Minimum input voltage, $(2E) = 200$ V,
Output voltage, $V_o = 100$ V,
Maximum load current = 5 A,
Switching frequency, $f_t = 100$ kHz.

Calculations show that the peak inductor current decreases for higher values of M and for switching frequencies near series resonance. The value chosen for the above example was $M = 1.2$ and $y = 1.1$. Corresponding to this point, the values of J, J_{Lp} and m_{csp} are read from Fig. 4. The values obtained are

$J = 3.15$ p.u., $J_{Lp} = 5.63$ p.u., and $m_{csp} = 5.76$ p.u.

Using $Z_s = (L_s/C_s)^{1/2} = MJE^2/P_o$, (34)

value of Z_s can be obtained. Also,

$y = 2\pi f_t/w_s$ (35)

where $w_s = 1/(L_s C_s)^{1/2}$. (36)

Hence the above two equations can be solved for L_s and C_s and the values obtained in this case are

$L_s = 132.5$ μH and $C_s = 0.023$ μF.

Therefore, $C_t = 0.023$ μF.

The component stresses obtained are:
Peak inductor current, $I_{Lp} = 7.435$ A.

Peak voltage across C_s, $V_{csp} = 576$ V,

Peak voltage across C_t, $V_{ctp} = 100$ V.

5. EXPERIMENTAL RESULTS

Typical waveforms obtained from an experimental converter (operating above resonance) are presented in Figs. 5 and 6 for variations in the load resistance from $R_L \simeq 27$ ohms to $R_L \simeq 232$ ohms. Details of the experimental converter are given in Fig. 5. A bridge rectifier was directly connected across C_t without a hf transformer.

In all the waveforms, switching frequency was adjusted to regulate the load voltage at approximately 93 V with variations in the load. It can be observed that mode-1 is the predominant mode as observed in Figs. 5 and 6(a). Mode-2 operation is illustrated in Fig. 6(b). Fig. 6(c) shows the waveforms for mode-3. These results confirm the theory and show that modes 2 and 3 occur for less than 25% load current. It is also observed that the inductor peak current, peak capacitor voltage across C_s, and the efficiency at different load conditions were comparable to those obtained with an inductive output filter. The peak capacitor voltage across C_t is less in the proposed converter.

6. CONCLUSIONS

A series-parallel resonant converter using a capacitive output filter has been proposed and analysed using state-space approach. Analysis shows that the converter operates in three modes. Steady-state solutions have been obtained for the different modes of operation based on the general solutions. Mode 1 was the predominant mode with operation in mode 3 occuring at light loads and higher switching frequencies. Design curves have been obtained based on the analysis and they have been used to illustrate the design procedure. Experimental results have been presented to verify the different modes of operation. A comparison of the proposed converter with a converter of same rating, but with inductive output filter shows that the peak inductor current and the peak voltage across C_s are almost the same for both. The peak voltage stress across C_t is much smaller in the new converter.

REFERENCES

1. K. Kit Sum, "Recent Developments in Resonant Power Conversion", Intertech Communications Inc., 1988.
2. A.K.S.Bhat and S.B.Dewan, "A generalized approach for the steady state analysis of resonant inverters", IEEE Transactions on Industry Appictaions, Vol. 25, No. 2, March/April 1989 pp. 326-338.
3. A.K.S. Bhat, "A Unified Approach for the Steady-State Analysis of Resonant Converters", International Conference on Power Electronics, Tokyo, pp. 191-197, April 1990.
4. R. Severns, "Topologies for Three Element Resonant Converters", IEEE Applied Power Electronics Conference Record, pp. 712-722 March 1990.

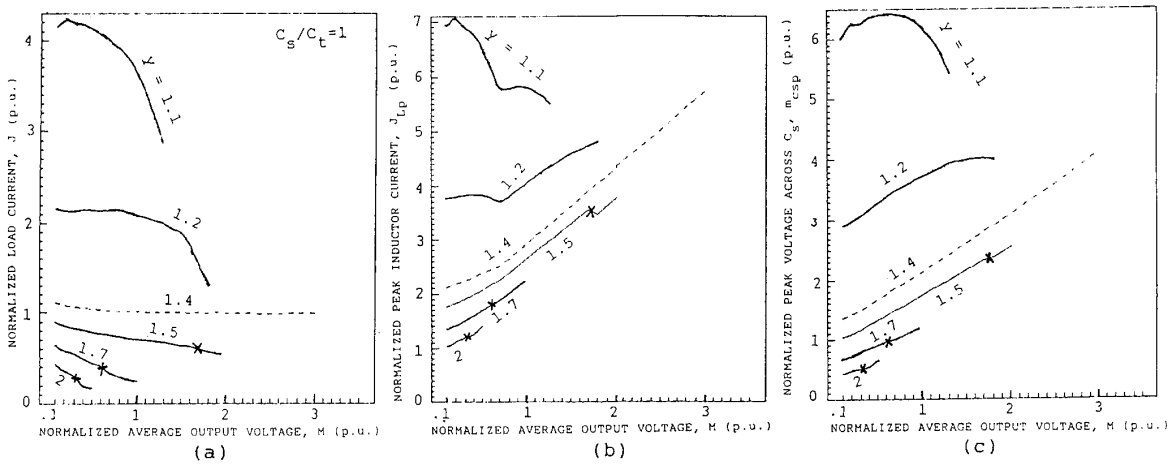

Fig. 4 Design curves obtained for C_s/C_t = 1:
(a) Normalized load current, J (p.u.),
(b) normalized peak inductor current, J_{Lp}, and
(c) normalized peak capacitor voltage across C_s, m_{csp}, versus normalized output voltage M (p.u.) (i.e. converter gain), for various values of y (ratio of triggering frequency to series resonane frequency). (Note that points marked with x correspond to mode 2 and the converter operates in mode 3 to the right of x).

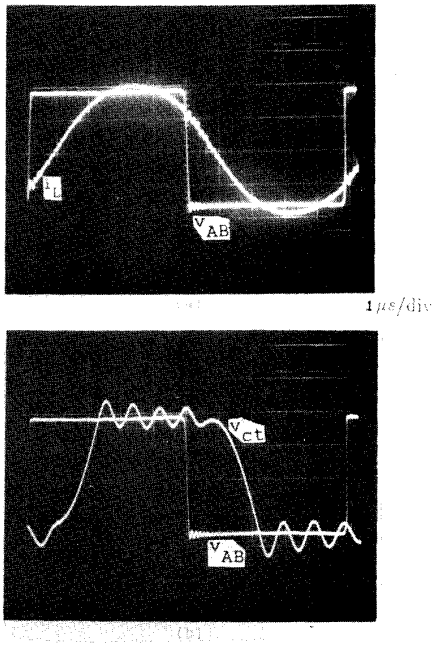

Fig. 5 Experimental results obtained with an experimental unit with $R_L \simeq 27$ ohms. (a) waveforms v_{AB} (50 V/div.) and inverter output current i_L (0.5 V/div., 1V = 5A), (b) voltage v_{AB} (50V/div.) and voltage across C_t (v_{ct}) (50 V/div.),

[Details of the converter : Switches used - MTM15N50 MOSFETs, Feedback diodes - internal to the MOSFETs, Input dc voltage = 200 V, $L_s \simeq 135$ μH, $C_s \simeq 0.0235$ μF, $C_t \simeq 0.0235$ μF]

5. R.L. Steigerwald, "A Comparison of Half-Bridge resonant converter topologies", IEEE transactions on Power Electronics, Vol. PE-3, No. 2, April 1988, pp. 174-182.
6. S.D. Johnson, A.F. Witulski and E.W. Erickson, "A Comparison of Resonant Topologies in High Voltage DC Applications", IEEE Applied Power Electronics Conference Record, 1987, pp. 145-156.
7. A.K.S. Bhat, "High Frequency Link Photovoltaic Power Conditioning System", M.A.Sc thesis, Dept. of Electrical Engineering, University of Toronto, Toronto, Sept. 1982.
8. J. Chen and R. Bonert, "Load Independent AC/DC Power Supply for High Frequencies With Sine-Wave Output", IEEE Tranasactions on Industry Applications, Vol. IA-19, No. 2, pp. 223-227, March/April 1983.
9. A.K.S.Bhat and S.B.Dewan, "Analysis and design of a high-frequency converter using LCC-type commutation", IEEE Transactions on Power Electronics, Oct. 1987, Vol. PE-2, No. 4, pp. 291-301.
10. A.K.S. Bhat and S.B. Dewan, "Steady-State Analysis of a LCC-Type Commutated High-Frequency Inverter", IEEE Power Electronics Specialists Conference Record, 1988, pp. 1220-1227.
11. R. Bonert and P. Blanchard, "Design of a Resonant Inverter With Variable Voltage and Constant Frequency", IEEE IAS Conference Record, 1988, pp. 1003-1008.
12. A.K.S. Bhat, "A Resonant Converter Suitable for 650V DC Bus Operation", IEEE Applied Power Electronics Conference Record, 1989, pp. 231-239.
13. I. Batarseh, R. Liu, C.Q. Lee and A.K. Upadhyay, "150 Watts and 140 kHz Multi-Output LCC-Type Parallel Resonant Converter", IEEE Applied Power Electronics Conference Record, 1989, pp. 221-230.
14. I. Batarseh, R. Liu, and C.Q. Lee, "Design of Parallel Resonant Converter with LCC-Type Commutation", Electronics Letters, Vol. 24, No. 3, Feb. 1988, pp. 177-179.
15. I. Batarseh, R. Liu, and C.Q. Lee, "High-Frequency High-Order Parallel Resonant Converter" IEEE Transactions on Industrial Electronics, Vol. 36, No. 4, Nov. 1989, pp. 485-498.
16. P.K. Jain, "Performance Comparison of Pulse Width Modulated Resonant Mode DC/DC Converters for Space Applications", IEEE IAS Conference Record, 1989, pp. 1106-1114.
17. A.K.S. Bhat, "Fixed Frequency PWM Series-Parallel Resonant Converter", IEEE IAS Conference Record, Oct. 1989, pp. 1115-1121.
18. A.K.S. Bhat, "Analysis, Optimization and Design of a Series-Parallel Resonant Converter", IEEE Applied Power Electronics Conference Record, pp. 155-164, March 1990.
19. K.D.T. Ngo, R.L. Steigerwald, A.J. Yerman and M.H. Kuo, "A High-Density Resonant Power Supply Using High-Voltage IC", HFPC Conference Record, April 1987, pp. 244-257.
20. Jones, D.V., "A New Resonant Converter Topology", HFPC Conference Record, April 1987, pp. 48-53.
21. Fischer, Korman, et al, "Performance of Low Loss Synchronous Rectifiers In a Series-Parallel Resonant Converter", IEEE Applied Power Electronics Conference Record, 1989, pp. 240-246.
22. Carsten, B., "A Hybrid Series-Parallel Resonant Converter for High Frequencies and Power Levels", HFPC Conference Record, pp. 41-47.

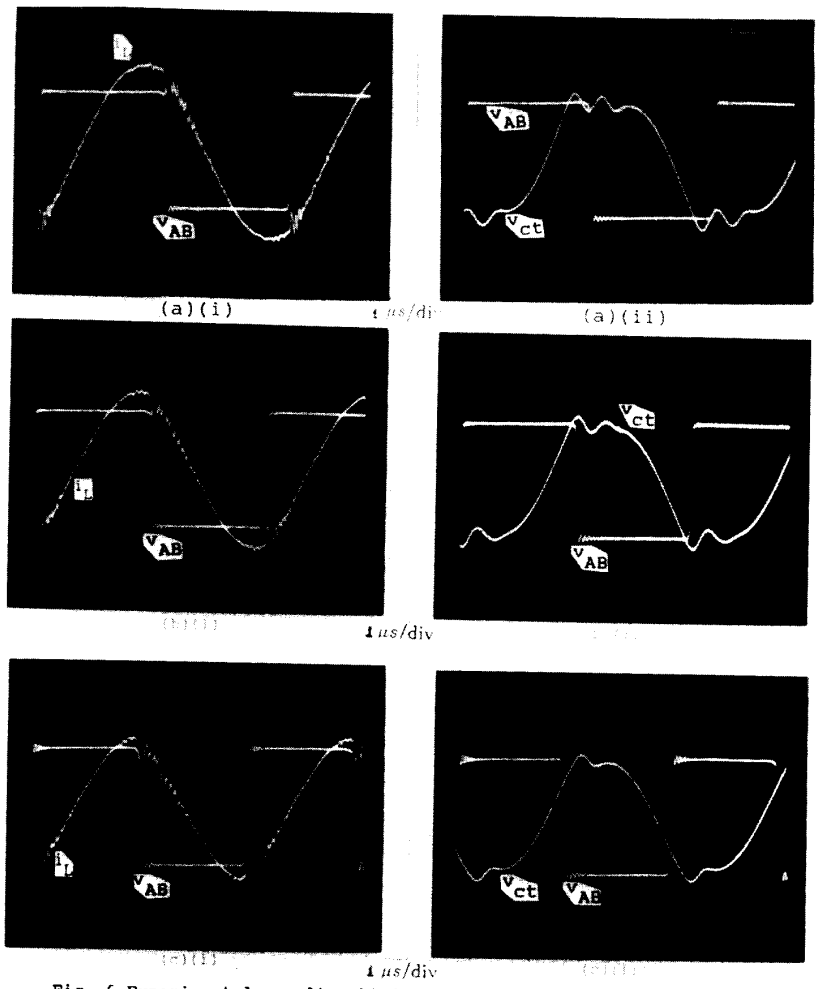

Fig. 6 Experimental results obtained with an experimental unit.
(a) With $R_L \simeq 48.8$ ohms: (i) waveforms v_{AB} (50 V/div.) and inverter output current i_L (0.2 V/div., 1V = 5A), (ii) v_{AB} (50V/div.) and v_{ct} (50V/div.)
(b) (i) and (ii) same as (a) with $R_L \simeq 120$ Ohms.
(c) (i) and (ii) same as (a) with $R_L \simeq 232$ Ohms.
[Details of the converter : Same as Fig. 5]

23. R.L. Steigerwald, "Analysis of a Resonant Transistor DC-DC Converter with Capacitive Output Filter", IEEE Transactions of Industrial Electronics, Vol. IE-32, No. 4, Nov. 1985, pp. 439-444.
24. S.D. Johnson and R.W. Erickson, "Steady-State Analysis and Design of the Parallel Resonant Converter", IEEE Transactions on Power Electronics, Vol. 3, No. 1, Jan. 1988, pp. 93-104.
25 S. Sooksatra and C.Q. Lee, "Series Resonant Converter with Inductive Filter", IEEE IAS Conference Record, 1989, pp. 1135-1140.

APPENDIX 1.
GENERAL SOLUTIONS OF MODE-1.

The normalized general solutions obtained for mode-1 during different intervals are (note that j_L represents the normalized inductor current, m_{cs} and m_{ct} represent the normalized voltages across the capacitors C_s and C_t, respectively):

Interval 1, $0<t<t_1$

$$j_L = (1-m_{ct0}-m_{cs0})\sin(w_s t) + j_{L0}\cos(w_s t) \quad \text{(A1.1)}$$

$$m_{cs} = (1-m_{ct0})-(1-m_{ct0}-m_{cs0})\cos(w_s t)+j_{L0}\sin(w_s t) \quad \text{(A1.2)}$$

$$m_{ct} = m_{op} \quad \text{(A1.3)}$$

where $m_{op} = m_{ct0}$

$= -M$ for above resonance,
$= M$ for below resonance.

Interval 2, $0<t'<t_2$

$$j_L = (1-m_{cs1}-m_{ct1})(C_e/C_s)^{1/2}\sin(w_e t') \quad \text{(A1.4)}$$

$$m_{cs} = (C_e/C_s)(1-m_{ct1}-m_{cs1})(1-\cos(w_e t') + m_{cs1} \quad \text{(A1.5)}$$

$$= (C_t/C_s)(m_{ct} - m_{ct1}) + m_{cs1} \quad \text{(A1.5a)}$$

$$m_{ct} = (C_e/C_t)(1-m_{ct1}-m_{cs1})(1-\cos(w_e t') + m_{ct1} \quad \text{(A1.6)}$$

where $m_{ct1} = -M$ for operation above resonance,
$= M$ for operation below resonance.

Interval 3, $0<t''<t_3$

$$j_L = (1-m_{ct2}-m_{cs2})\sin(w_s t'') + j_{L2}\cos(w_s t'') \quad \text{(A1.7)}$$

$$m_{cs} = (1-m_{ct2}) - (1-m_{ct2}-m_{cs2})\cos(w_s t'') + j_{L2}\sin(w_s t'') \quad \text{(A1.8)}$$

$$m_{ct} = m_{op} \quad \text{(A1.9)}$$

where $m_{op} = m_{ct2}$

= M for operation above resonance,
= -M for operation below resonance.

APPENDIX 2.
GENERAL SOLUTIONS OF MODE 2.

There are only two intervals, 1 and 2, for this mode of operation. The general solutions given for the first two intervals of mode 1 are valid for this mode also.

APPENDIX 3.
GENERAL SOLUTIONS OF MODE 3.

The normalized general solutions of mode 3 (Fig. 3(c)) are presented below.

Interval 1, $0<t<t_1$

$$j_L = (C_e/C_s)^{1/2}(1-m_{ct0}-m_{cs0})\sin(w_e t)+j_{L0}\cos(w_e t) \quad \text{(A3.1)}$$

$$m_{cs} = (C_e/C_s)(1-m_{ct0}-m_{cs0})(1-\cos(w_e t)) + (C_e/C_s)^{1/2} j_{L0}\sin(w_e t) + m_{cs0} \quad \text{(A3.2)}$$

$$m_{ct} = (C_e/C_t)(1-m_{ct0}-m_{cs0})(1-\cos(w_e t)) + (C_s/C_t)(C_e/C_s)^{1/2} j_{L0}\sin(w_e t) + m_{ct0} \quad \text{(A3.3)}$$

Interval 2, $0<t'<t_2$

$$j_L = (1-m_{cs1}-m_{ct1})\sin(w_s t') + j_{L1}\cos(w_s t') \quad \text{(A3.4)}$$

$$m_{cs} = (1-m_{ct1})-(1-m_{ct1}-m_{cs1})\cos(w_s t')+j_{L1}\sin(w_s t') \quad \text{(A3.5)}$$

$$m_{ct} = m_{ct1} \quad \text{(A3.6)}$$

where m_{ct1} = -M for operation above resonance,
= M for operation below resonance.

Interval 3, $0<t''<t_3$

$$j_L = (C_e/C_s)^{1/2}(1-m_{ct2}-m_{cs2})\sin(w_e t'') \quad \text{(A3.7)}$$

$$m_{cs} = (C_e/C_s)(1-m_{ct2}-m_{cs2})(1-\cos(w_e t'')) + m_{cs2} \quad \text{(A3.8)}$$

$$m_{ct} = (C_e/C_t)(1-m_{ct2}-m_{cs2})(1-\cos(w_e t'')) + m_{ct2} \quad \text{(A3.9)}$$

where m_{ct2} =-M for operation above resonance,
= M for operation below resonance.